A&A 603, A26 (2017)
DOI: 10.1051/0004-6361/201629415

Astronomy & Astrophysics

New eruptive variable in the massive star-forming region associated with IRAS 18507+0121

E. H. Nikoghosyan, N. M. Azatyan, and K. G. Khachatryan

Byurakan Astrophysical Observatory, 0213 Aragatsotn Prov., Armenia
e-mail: elena@bao.sci.am

Received 28 July 2016 / Accepted 24 March 2017

ABSTRACT

Aims. We report the discovery of a strong outburst of the embedded young stellar object (YSO) UKIDSS−J185318.36+012454.5, located in the star-forming region associated with IRAS 18507+0121 and the ultra-compact H II region GAL 034.4+00.23.
Methods. Using archival photometric data and images, we determined the amplitude and the epoch of the outburst as well as the evolution stage and the basic parameters of the object.
Results. According to the near- and mid-infrared colors and spectral energy distribution, we classify the object as an intermediate-mass YSO with Class 0/I evolution stage. The outburst apparently started between May 2003 and April 2004. The amplitude of the outburst is at least $\Delta K_s = 5.0$ mag. The summation of the photometric and spectral data does not allow classifying UKIDSS−J185318.36+012454.5 as an FU Orionis (FUor) or EX Orionis (EXor) object. We can consider it as an eruptive variable with mixed characteristics or as an MNor type object.

Key words. infrared: stars – stars: pre-main sequence – stars: individual: UKIDSS-J185318.36+012454.5

1. Introduction

Eruptions of pre-main sequence (PMS) stellar objects are rare events, therefore a new outburst is always noteworthy. This topic has always been in the spotlight of observers and theorists. Nevertheless, the number of verified eruptive variable PMS stars remains too small. However, as a result of significant developments of infrared observations that allow us to penetrate in embedded and distant star-forming regions, there has been some progress in this regard (Scholz et al. 2013; Contreras Peña et al. 2014, 2017). Most solar-like eruptive variable young stellar objects (YSOs) have been divided into two subclasses: FU Orionis (FUors) and EX Orionis (EXors). FUor-type eruptive variables show a larger increase of luminosity (up to 6 mag) and slow decay over >10 yr (Hartmann & Kenyon 1996). This class of objects generally displays strong CO and H_2O absorption and mostly lack of emission lines in their infrared spectra. EXor-type variables have recurrent short-lived (as rule <1 yr) outbursts (Herbig 2008). In contrast with FUors, a strong Brγ and CO emission dominates during the outburst in the infrared spectrum of EXors. This optically defined classification does not include the young embedded protostars that have a higher accretion rate and a mixture of characteristics. For this class of YSOs, the relatively new label MNOrs has been proposed (Contreras Peña et al. 2014).

We report the discovery of the new embedded eruptive variable YSO UKIDSS−J185318.36+012454.5 (DR6 release of the UKIDSS GPS survey). The stellar object is located in the massive star-forming region associated with IRAS 18507+0121. In the vicinity of IRAS, the ultra-compact (UC) H II region G034.4+00.23 was discovered, which is embedded in the filamentary dark molecular cloud MSXDC G034.43−00.24 (Miralles et al. 1994). UKIDSS−J185318.36+012454.5 is also identified in the rms archive as G034.4035+00.2282A (Lumsden et al. 2013). Continuum dust emission, traced by millimeter and submillimeter images, revealed four compact clumps in this star-forming region, MM11-MM4 (Rathborne et al. 2005). One of them, MM2, coincides with the IRAS 18507+0121 star-forming region. The G034.43−00.24 MM2 clump is also traced by $H^{13}CO^+$, SiO, and 6 cm emission (Harju et al. 1998; Shepherd et al. 2004, 2007). Different manifestations of star-forming activity are detected in the region. The IRAS 18507+0121 region is associated with variable H_2O (Miralles et al. 1994), CH_3OH (Szymczak et al. 2000), OH (Edris et al. 2007), and NH_3 (Molinari et al. 1996) maser emission. Three massive molecular outflows are centered on or near G34.4+0.23 (Shepherd et al. 2007). The outflow is also detected in mid-infrared wavelengths (Shepherd et al. 2007; Cyganowski et al. 2008).

The stellar population was studied, and some massive protostars with an age of $\sim 10^5$ yr have been identified in this star-forming region, as well as a low-mass stellar population with an age of $\sim 10^6$ yr (Shepherd et al. 2007). Shepherd and collaborators suggested that the stars in this region may have formed in two stages: first, lower mass stars were formed, and then more massive stars began to form. UKIDSS−J185318.36+012454.5 is located at a distance ∼3″ in the NW direction from the luminous source (IR source #54 in Shepherd et al. 2004). In the immediate vicinity of IRAS 18507+0121, a compact group of YSOs (including UKIDSS−J185318.36+012454.5) was revealed (Morales et al. 2013; Azatyan et al. 2016).

The distance estimates of G34.4+0.23 are very contradictory. VLBI parallax measurements of H_2O maser sources within the infrared dark cloud MSXDC G034.43+00.24 determined a distance of 1.56 kpc (Kurayama et al. 2011). The estimates of the kinematic distance considerably exceed the previous value and

Table 1. NIR photometric data.

Source	Date of obs.	H [mag]	K_s [mag]
2MASS	1999−08−10	–	–
DENIS	2000−07−03	–	–
Varricatt et al. (2010)	2003−05−27	–	$K_s \geq 18.5$
DR6 UKIDSS GPS	2006−06−01	17.07 ± 0.04	13.76 ± 0.01
Cooper et al. (2013)	2007−06−02	17.20 ± 0.30	13.76 ± 0.08
SOFI (ID 083.C−0846)	2010−06−05	–	13.68 ± 0.10
DR9 UKIDSS GPS	2011−08−11	–	13.75 ± 0.03

vary from 3.7 kpc (Simon et al. 2006) to 3.9 kpc (Molinari et al. 1996). Although a parallax measurement would seem to be a more reliable distance determination, Foster et al. (2012) suggested that the parallax determinations to the same sources are incorrect because of the low declination of this target.

In this paper we present evidence of the outburst, that occurred in YSO UKIDSS−J185318.36+012454.5 or G034.4035+00.2282A. We have defined the amplitude and the epoch of the outburst, as well as an evolution stage and the basic parameters of the stellar object.

2. Observations

To identify and study the eruptive variable UKIDSS−J185318.36+012454.5, we acquired archival infrared and submillimeter data and images. For the near-IR (NIR) bands the photometric data from DR6 of UKIRT Galactic Plane Survey (UKIDSS GPS, Lucas et al. 2008) and Cooper et al. (2013) were employed. We also used the K images from the ESO archive (SOFI infrared imager/spectrometer Moorwood et al. 1998), DR9 release of UKIDSS GPS and Varricatt et al. (2010).

For the Mid-IR (MIR) bands, we acquired IRAC data (Fazio et al. 2004) from the *Spitzer* Science Archive, which include the photometric parameters obtained from GLIMPSE I (Benjamin et al. 2003; Churchwell et al. 2009) and DEEP GLIMPSE (Whitney et al. 2011) catalogs. In addition, for photometric measurements we used [3.6] and [4.5] band images obtained from programs with AOKEYs 42718976, 10291200 and 42728960.

Photometric measurements were made according to the standard procedure using the aperture photometry package APPHOT in IRAF. The zero-point fluxes of the [3.6] and [4.5] bands (Vega-standard magnitudes for 1 DN s^{-1}) were adopted from Reach et al. (2005).

We also used data from 2MASS (Skrutskie et al. 2006), DENIS (Epchtein et al. 1999), AKARI (Ishihara et al. 2010) and Hi-GAL (Molinari et al. 2016) surveys, as well as from rms archive (Lumsden et al. 2013).

3. Results

3.1. Luminosity variability

The photometric data and images of UKIDSS−J185318.36+012454.5 in the NIR bands taken at different epochs are presented in Table 1 and Fig. 1 respectively. They show that the stellar object was not identified in 2MASS and DENIS surveys. Therefore, its brightness in 1999 and 2000 was fainter than K_s = 18 mag. Additionally, it is necessary to note that in K image in Shepherd et al. (2004) which was obtained in 1999, the object also was invisible. In the K_s images, which are obtained with higher sensitivity with the United Kingdom Infrared Telescope in 2003, the stellar object is barely noticeable as the nebulous knot, the surface brightness of which does not exceed 18.5 mag. Then, during 2003–2006, the luminosity of the object strongly increased, at least by 5 mag in K_s band, and reached ∼13.75 mag. The object brightness remained practically unchanged until 2011.

A noticeable increase in brightness is also observed in MIR range. The photometric data are presented in Table 2 (see also Fig. 1). The first measurements were obtained in 2004, before the outburst detection in the K band. After that, the photometric data cover a later period from 2012 untill 2014 and indicate that the brightness increased by ∼1 mag in [3.6] μm and ∼0.5 mag in [4.5] μm the bands. We did not consider the MIPSGAL 24 μm data because the immediate vicinity of the UC H II region is saturated, as the majority of rms sources, which does not allow photometric measurements. It should be noted that all photometric data, which cover a period from 2006 to 2014, show that within the error bars, the object brightness remained practically at the same level and underwent only insignificant fluctuations.

Unfortunately, the spatial resolution of longer wavelength images does not allow exact measurements of the fluxes in different wavelengths and epochs. For example, in Fig. 2 we overplot K_s band image (UKIDSS GPS) and isophotes of sources from MSX (21 μm), WISE 4 (22 μm), SCUBA (850 μm), and ATLASGAL (870 μm) surveys. These sources virtually cover the central part of MM2 clump (Rathborne et al. 2005), which includes a number of YSOs that overlie the UC H II region. This produces bright diffuse emission in MIR and far-IR (FIR) bands (Shepherd et al. 2004, 2007; Lumsden et al. 2013). It is therefore not possible to determine the exact values of fluxes in different wavelengths separately for the objects. The effect of the outburst on the total flux in the longer wavelengths can be insignificant. In Fig. 3, we present the broadband continual spectral energy distributions (SEDs) of data obtained before 2003 and after 2006 yr. We obtained the photometric data from the rms archive and from the AKARI and Hi-GAL surveys. For the earlier epoch before the outburst, we used data from MSX (1996), IRAS (1983), SCUBA (2000), and SIMBA/MAMBO (2001–2002), which cover the wavelength range from 8 μm to 1.2 mm. Although the coordinates of IRAS 18507+0121 according to the IPAC data are significantly offset from MSX source (∼18″, see Fig. 1), its fluxes were also used. We were guided by the corrected coordinates of the IRAS source from the IRAS PSC/FSC Combined Catalogue (Abrahamyan et al. 2015), whose offset from the MSX source is only ∼1.5″. For the later period after the outburst, the data of WISE 12 μm and 22 μm (2010), AKARI (2007), MIPS 70 μm (2010), ATLASGAL (2007), BGPS (2007), and Hershel PACS (2011) were used. They cover practically the same wavelength range from 9 μm to 1.1 mm. There is an insignificant difference between the integral fluxes obtained in different epochs. In total, the flux of the later period increased by ∼10%, which only slightly exceeds or is comparable to the error

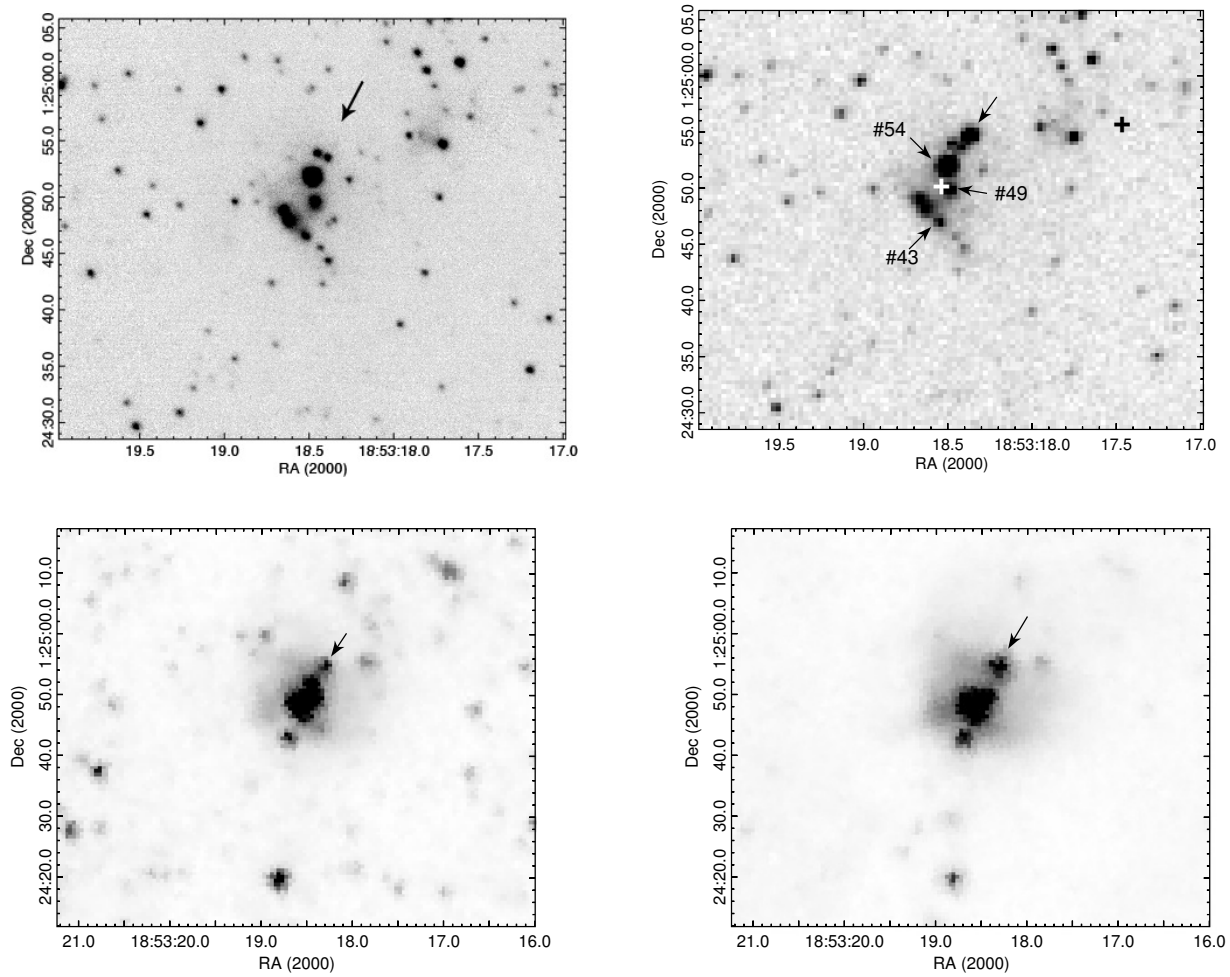

Fig. 1. UKIDSS−J185318.36+012454.5 in different wavelengths: K_s band from Varricatt et al. (2010; *left top*), K_s band from DR6 UKIDSS GPS (*right top*), [3.6] μm band from the GLIMPSE I survey (*left bottom*), and [5.8] μm band from the GLIMPSE I survey (*right bottom*). The coordinates of IRAS 18507+0121 from the IRAS PSC and IRAS PSC/FSC Combined Catalogue (Abrahamyan et al. 2015) are marked by black and white crosses, respectively. In the DR6 UKIDSS GPS K_s image, three stellar sources are marked (#43, #49 and #54, Shepherd et al. 2004), for which we present in Table 3 the photometric data (a more detailed description is given in the text).

Table 2. MIR photometric data.

Source	Date of obs.	[3.6] [mag]	[4.5] [mag]	[5.8] [mag]	[8.0] [mag]
GLIMPSE I	2004−04−23	11.55 ± 0.35	9.62 ± 0.18	7.8 ± 0.01	6.65 ± 0.09
DEEP GLIMPSE	2012	10.56 ± 0.11	9.10 ± 0.04	–	–
AOKEY 4218976	2012−06−09	10.35 ± 0.30	9.04 ± 0.20	–	–
AOKEY 10291200	2012−11−16	10.54 ± 0.30	9.10 ± 0.20	–	–
AOKEY 42728960	2014−12−13	10.24 ± 0.30	9.41 ± 0.20	–	–

bars of the photometric data and it cannot be regarded as clear evidence of the outburst.

The effect of the outburst on the total flux from UC H II region is more noticeable by comparing the data obtained in different epochs from relatively equivalent wavelength ranges and beam sizes or equivalent radii, such as MSX E and WISE 4 fluxes. The flux of MSX E band (21 μm, beam size of 18.3″) is 13.6 ± 0.8 Jy. The flux of the WISE 4 band (22 μm, bean size of 12″) is 17.6 ± 0.2 Jy. The offset between the coordinates is ∼1″. Therefore, the flux at 21–22 μm within this area increased by ∼4 Jy or 23% during the period 1996–2010. When we assume that only UKIDSS-J185318.36+012454.5 is variable, then the derived value should provide an estimate of its flux variability at MIR wavelengths. According to the rms survey, there are two YSOs and an UCHII emitting region associated with the MSX emission from G034.4035+00.2282. One of them is UKIDSS−J185318.36+012454.5 or G034.4035+00.2282A. According to Lumsden et al. (2013), the fraction of this YSO in the total luminosity in MIR wavelength is ∼0.2, which is comparable with the difference between the MSX E and WISE 4 fluxes.

The increase in brightness can also be seen in a longer wavelength bands. The flux of the SCUBA 850 μm (R_{ef} = 52″) source is 21.7 ± 4.3 Jy. The flux of the ATLASGAL 870 μm (R_{ef} = 40″) source is about twice higher and equal to 40.5 ± 6.4 Jy. The offset between the peak coordinates is ∼5.5″. The peak fluxes in both

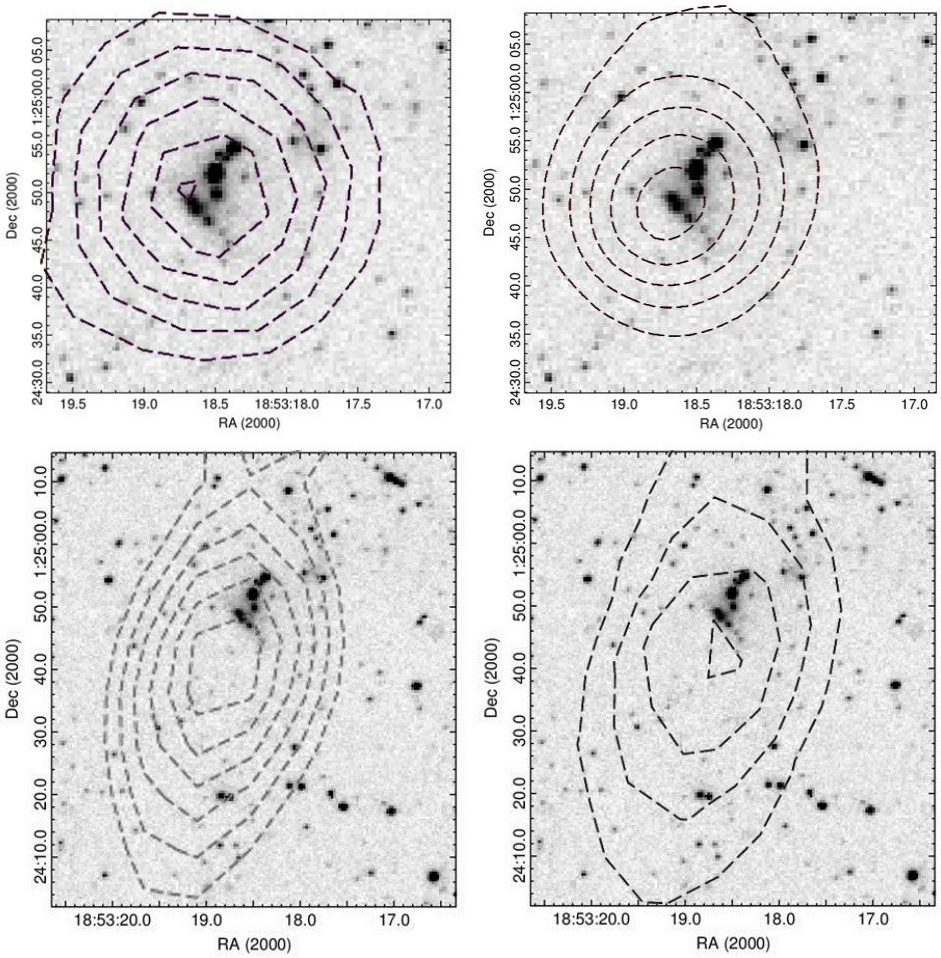

Fig. 2. K_s band image overplotted with isophotes of MSX 21 μm (*left top*), WISE 22 μm (*right top*), SCUBA 850 μm (*left bottom*), and ATLASGAL 870 μm (*right bottom*) sources.

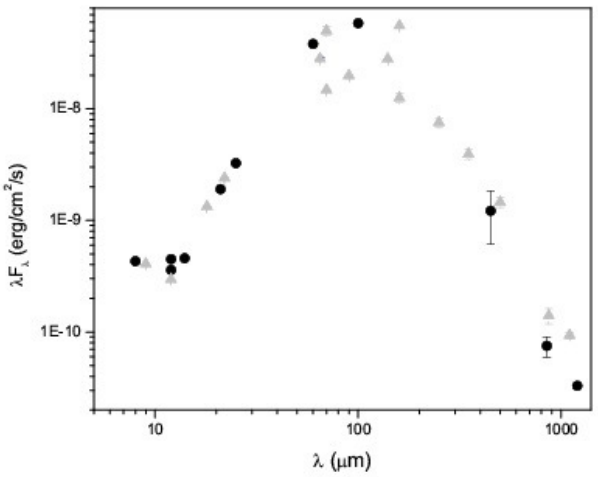

Fig. 3. Broadband continuum SED of the HII region G034.4035+00.2282: the data obtained before 2003 (MSX, IRAS, SCUBA, and SIMBA/MAMBO) are marked by black circles, the data obtained after 2006 (WISE 12 μm and 22 μm, AKARI, *Spitzer* MIPS, ATLASGAL, BGPS and *Herschel* PACS) are marked by gray triangles.

databases are the same and equal to 7.4 Jy/beam. Nevertheless, from our point of view, the rising of the submillimeter flux, integrated over such a large area, can only be regarded as indirect evidence of the outburst.

In order ensure that such a significant increase in the brightness of UKIDSS−J185318.36+012454.5 is not caused by the variability in the extinction along the line of sight, we determined the K_s magnitudes of stars that are located in the immediate vicinity. They are marked in Fig. 1. All objects are identified in Shepherd et al. (2004) and the UKIDSS GPS survey. The NIR photometric data of the neighboring stars are presented in Table 3. In addition to magnitudes from the UKIDSS GPS database, we determined their K_s magnitudes in images acquired from Varricatt et al. (2010). Between these two epochs, a significant brightness increase of UKIDSS−J185318.36+012454.5 was detected. As seen from the data in Table 3, the brightness variability of nearby stars is not significant and does not exceed ∼0.5 mag. This can be seen as an argument in favor of the fact that such a significant brightness increase of UKIDSS−J185318.36+012454.5 did not occur as a result of the extinction variability towards the star-forming region.

This conclusion is also supported by the MIR photometric data. According to the relations presented in Xue et al. (2016), the extinction at 22.09 μm (WISE band 4) relative to that at 2.16 μm (Ks band) is $A(W4)/A(Ks) \approx 0.364$. If the luminosity variation in Ks band ($\Delta Ks \approx 5$ mag) is due to a change of extinction toward the source, we can expect that ΔW4 will be ∼1.8 mag. However, as mentioned above, the flux in 21–22 μm increased by ∼4 Jy, which corresponds only to ∼0.3 mag. Therefore we can exclude extinction as the main cause of the observed variability and confirm that the latter is due to an accretion burst.

Table 3. H and K_s magnitudes of nearby stellar objects.

Object	Varricatt et al. (2010)	DR6 UKIDSS GPS	
	K_s [mag]	H [mag]	K_s [mag]
(#54) UKIDSS−J185318.49+012451.8	12.55 ± 0.03	13.67 ± 0.01	12.55 ± 0.01
(#49) UKIDSS−J185318.48+012449.6	14.72 ± 0.04	–	14.29 ± 0.01
(#43) UKIDSS−J185318.46+012446.8	15.21 ± 0.04	17.83 ± 0.07	14.83 ± 0.01

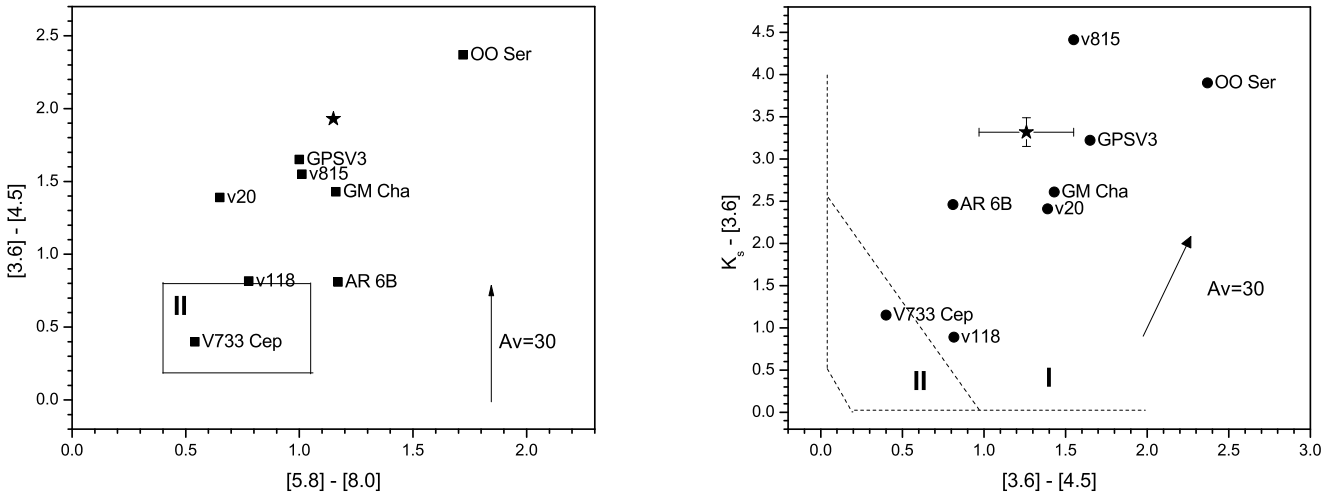

Fig. 4. Classification of UKIDSS−J185318.36+012454.5 and other eruptive variables using NIR and MIR measurements. In *the left panel*, the rectangle marks the domain of Class II sources. The Class I domain is above and to the right (Allen et al. 2004). In the *right panel* the colors are separated into Class I and II domains by the diagonal dashed line (Gutermuth et al. 2008). Arrows show extinction vectors for $A_V = 30$ (Rieke & Lebofsky 1985; Flaherty et al. 2007). The position of UKIDSS−J185318.36+012454.5 marked by a star. In the *right panel* the average magnitudes from Tables 1 and 2 are used. The error bars are equal to the standard deviation.

We can consider UKIDSS−J185318.36+012454.5 as an eruptive variable.

3.2. Evolutionary stage

Figure 4 shows the two-color diagrams where we mark the positions of UKIDSS−J185318.36+012454.5 according to the NIR and MIR photometric data obtained in 2004 and after 2006 (see Tables 1 and 2). The position of the object in the [3.6]–[4.5] versus [5.8]–[8.0] colors diagram allows us to classify the object as a Class 0/I YSO (Hartmann et al. 2005). After the brightness increase in the MIR range [3.6]–[4.5], the color becomes bluer, which is reflected in the K − [3.6] versus [3.6]–[4.5] colors diagram. In this diagram, the object occupied the position of a Class I YSOs.

For comparison, we mark in the diagrams the positions of other eruptive variables. The colors of our object are comparable with those of the deeply embedded stellar sources AR 6B, OO Ser and GM Cha (Aspin & Reipurth 2003; Hodapp et al. 1996; Persi et al. 2007), which, based on their SEDs, are classified as Class I eruptive variable YSOs (Gramajo et al. 2014). In addition, the positions of the deeply embedded eruptive variables GPS V3, VVVv20, and VVVv815, which are also classified as Class I YSOs with an age of $\sim 10^5$ yr, (Contreras Peña et al. 2014, 2017) are marked in the diagram. We note that VVVv118 (Contreras Peña et al. 2014) with an age of $\sim 10^6$ yr and V733 Cep, which is not surrounded by a cool envelope (Reipurth et al. 2007), occupy the positions of a Class II PMS objects.

The estimates of the interstellar extinction (A_v) in G034.4035+00.2282 vary from $A_v = 20$ mag (Shepherd et al. 2004) to $A_v = 29$ mag (COBE/DIRBE and IRAS/ISSA maps (Schlegel et al. 1998)). According to the data of observations in the $C^{18}O$ line $N_{H2} = 2.4 \times 10^{22}$ (Xu et al. 2016). Therefore, as evident from the conversion factor between column density and interstellar extinction, $N_{H2} = 9.4 \times 10^{20}$ cm^{-2} A_v/mag ($R_v = 3.1$, Bohlin et al. 1978) $A_v = 25.5$ mag. Apparently, $A_v \approx 30$ mag is the upper limit of extinction in this region. We note that even we take the upper limit of an interstellar extinction into account, the colors of UKIDSS−J185318.36+012454.5 correspond to a Class I YSOs.

Combining all the available NIR and MIR measurements (H, K, [3.6], [4.5], [5.8], [8.0] and WISE 4), we have constructed the SED of UKIDSS−J185318.36+012454.5 (see Fig. 5). For the flux in 22 μm, we used the difference between fluxes of the MSX E and WISE 4 bands (see text above). The SED of our object is exceptionally red in the 1.5 to 5 μm region, with H – [4.5] ≈ 8 mag. At longer wavelengths (from 5.8 to 8.0 μm, before the brightening in the MIR) the SED of the object becomes roughly flat. For comparison, the SEDs of other Class I embedded eruptive variables (OO Ser, GM Cha, GPS V3 and VVVv815) are plotted in Fig. 5. In the MIR range the SED shape of GM Cha, GPS V3, and VVVv815 are similar to that of UKIDSS−J185318.36+012454.5. At longer wavelengths, toward 22 μm, however, their SEDs decline. In this range, the SED of UKIDSS−J185318.36+012454.5 is similar to that of another embedded eruptive variable OO Ser. The slope of the SED ($\frac{\Delta\log(\lambda F_\lambda)}{\Delta\log(\lambda)}$) for the 4.5–22 μm range for UKIDSS−J185318.36 + 012454.5 is 1.9, and for OO Ser it is 1.7. For both objects, the photometric data were obtained after the outburst. We note that according to the data presented in Gramajo et al. (2014), the disk mass accretion rate of OO Ser is the highest of all Class I FUors.

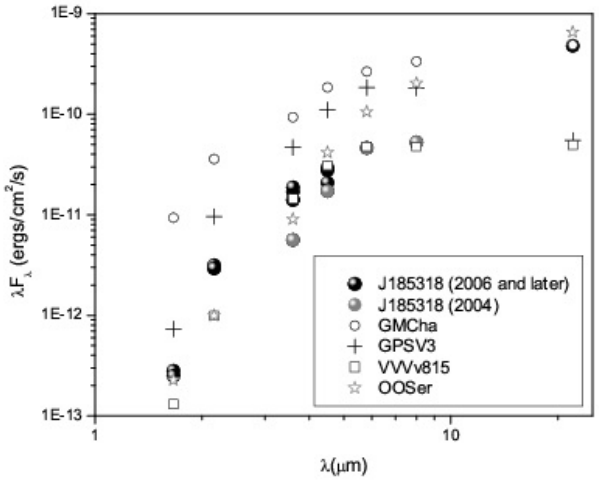

Fig. 5. SEDs of UKIDSS−J185318.36+012454.5, OO Ser, GM Cha, GPS V3 and VVVv815 eruptive variables. For UKIDSS−J185318.36+012454.5 all the photometric measurements from Tables 1 and 2 are marked. For 22 μm the differences of fluxes of MSX E and WISE 4 bands were used (a more detailed description is given in the text).

3.3. SED fitting analysis

Thus, according to the NIR and MIR photometric data, the stellar object UKIDSS−J185318.36+012454.5 can be classified as a YSO with a Class 0/I evolutionary stage and an age of $\leq 10^5$ yr (Lada & Lada 2003; Allen et al. 2007). The evolutionary stage and location in the direction to the central part of the MM2 clump of the UC H II region G034.4035+00.2282, where several protostars with an age of $\sim 10^5$ yr were revealed (Shepherd et al. 2004) suggests that the object belongs to this star-forming region. The estimations of the distance to this star-forming region are controversial. The trigonometric maser parallax distance is equal to 1.56 kpc (Kurayama et al. 2011). The kinematic distance considerably exceeds the previous value and varies from 3.7 kpc (Simon et al. 2006) to 3.9 kpc (Molinari et al. 1996). This greatly complicates the classification of the studied variable YSO.

To provide a rough estimate of the basic parameters of the object we used the SED fitting tool of Robitaille et al. (2007). For the SED fits, as in Sect. 3.2, we used the average NIR photometric data from Table 1, average magnitudes of the [3.6] and [4.5] bands obtained after brightening (after 2004, see Table 2), and magnitudes of the [5.8] and [8.0] bands obtained in 2004. The SED fitting tool might not be able to give distinct information for highly variable sources. In addition, the NIR and MIR photometric measurements are not contemporaneous. To minimize the problem, a 10% uncertainty was assumed for each band. For the 22 μm flux, we used the difference between the fluxes of the MSX E and WISE 4 bands. We fixed the distance ranges from 1.2 to 1.8 kpc and 3.0 to 5.0 kpc for the near and far estimates of the distance, respectively. As mentioned above, the estimates of the interstellar extinction (A_v) vary from 20 to 30 mag. We used some wider range from 10 to 40 mag for both cases. Figure 6 and Table 4 show the results obtained after using the SED fitting procedure.

To identify the representative values of different physical parameters, the tool retrieved the best-fit model, and all models for which the differences between their χ^2 values and the best χ^2 were smaller than $3N$, where N is the number of the data points (as suggested in Robitaille et al. 2007). This approach was taken because the sampling of the model grids is too sparse to effectively determine the minima of the χ^2 surface and consequently obtain the confidence intervals. Table 4 shows the values for different parameters corresponding to models with $\chi^2_{\rm best}$, as well as the weighted averages and the standard deviations of values for all models with $\chi^2 - \chi^2_{\rm best} < 3N$. We used 259 models for each target or the fitting degeneracy for near and 246 models for far distance estimates. The best-fitting model does not always represents the data very well (Grave & Kumar 2009). For the far variant, the estimates of the age, temperature, and total luminosity of the model with the best χ^2 are significantly lower than the weighted averages of models with $\chi^2 - \chi^2_{\rm best} < 3N$. The situation is similar for the value of a disk accretion rate for the near distance. The value of the best-fitting model is $\sim 10^3$ times lower than the weighted average.

As expected, the mass estimates according to the SED fitting tools for two variants of the distance differ significantly. However, in both cases we can classify UKIDSS−J185318.36+012454.5 as an intermediate-mass YSO with an age of $\leq 10^5$ yr. Even in the first case (near variant) the object exceeds by mass all Class I FUors from the list in Gramajo et al. (2014). The ratio between the mass, total luminosity, and age of our object, as well as the disk accretion and envelope infall rates, correlates well within the error bars with the several embedded eruptive variable YSOs presented in Contreras Peña et al. (2017). The objects VVV v20 and v815 are for nearer variant and VVV v405, v473, and v800 for the more distant variant. We note that about the same ratio between the envelope infall and disk accretion rates was also found for L1551 IRS 5 and GM Cha IR eruptive variables (Gramajo et al. 2014).

The value of the interstellar extinction (A_v) is correlated well with the previous estimates.

4. Discussion

The analysis of archival data allows us to reveal the new variable stellar object UKIDSS-J185318.36+012454.5, located in the massive star-forming region associated with UC H II region G034.4+00.23 and IRAS 18507+0121. The stellar object, according to the NIR and MIR colors and the SED, is a YSO with a Class 0/I evolutionary stage. In the NIR images obtained in 1999, 2000, and 2003 the object was indistinguishable. Since 2006, the object brightness drastically increased. The brightness amplitude increased during 2003–2006 by at least $\Delta Ks = 5.0$ mag. At this level of brightness, with insignificant fluctuations, UKIDSS-J185318.36+012454.5 remained at least until 2011. We note that even after the outburst, the object was invisible in J band. The earliest MIR images of the object were obtained in 2004. The subsequent observations during the period of 2012–2014 showed that the brightness of the object increased by ~1 mag in [3.6] band. The brightness variability in the [4.5] band was significantly lower and did not exceed 0.5 mag. The brightness variability was also detected at longer wavelengths. The flux associated with G034.4+00.23 region of the WISE 4 source (2010) increased compared with the flux of the MSX E source (1996) by ~4 Jy.

Several physical mechanisms, such as rotation, cool or hot spots (Scholz et al. 2009), accretion-driven wind, and outflow (Bans & Königl 2012) can explain the NIR variability observed in YSOs. However, these mechanisms often produce short-term variability with an amplitude that is not expected to exceed 1 mag in K band. The same physical processes produce the variability in MIR bands (Vijh et al. 2009). As a rule, however, this type of variability does not exceed 0.6 mag. Infrared variations

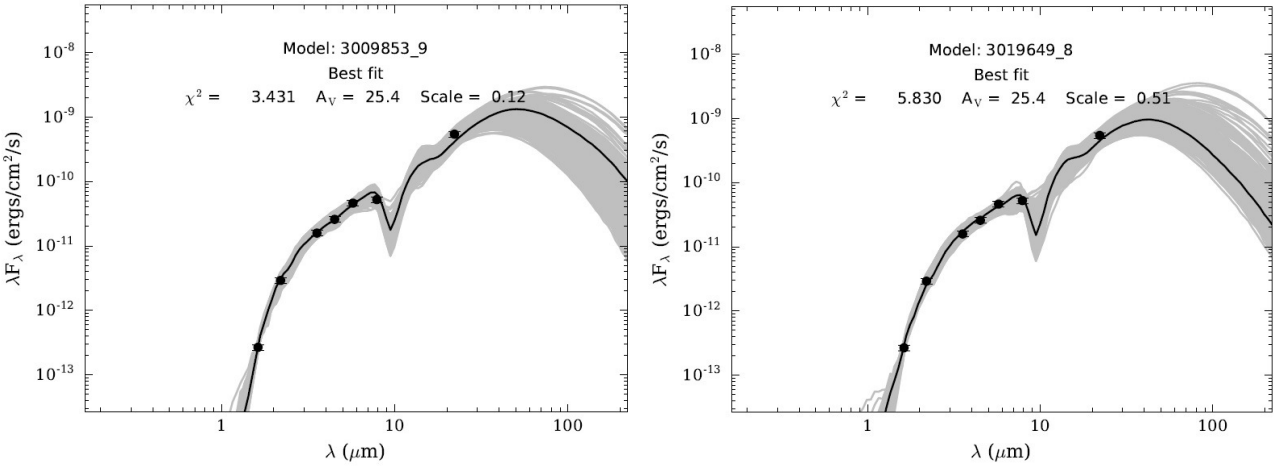

Fig. 6. Observed SED and the best-fit models for the distance range from 1.2 to 1.8 kpc (*left panel*) and from 3.0 to 5.0 kpc (*right panel*). Filled circular represent the data points.

Table 4. Parameters derived from Robitaille et al. (2007) model SED fitting.

Parameter	D = 1.2–1.8 kpc		D = 3.0–5.0 kpc	
	$\chi^2_{\rm best}$ = 3.4	χ^2–$\chi^2_{\rm best} < 3N$	$\chi^2_{\rm best}$ = 5.83	χ^2–$\chi^2_{\rm best} < 3N$
A_v [mag]	25.4	29.8 ± 4.0	25.4	29.0 ± 4.0
D [kpc]	1.32	1.47 ± 0.04	3.21	3.94 ± 0.55
Age (10^5 yr)	0.64	0.74 ± 0.33	0.24	1.55 ± 0.8
Stellar mass [$M_\odot$]	3.88	3.97 ± 0.60	7.52	7.44 ± 1.02
T [K]	4430	4700 ± 670	4530	8790 ± 2287
Total luminosity [$L_\odot$]	111	158 ± 36	547	1170 ± 304
Disk accretion rate (10^{-5} $M_\odot$ yr^{-1})	2.6e−4	0.15 ± 0.12	1.3	1.0 ± 1.34
Envelope infall rate (10^{-5} $M_\odot$ yr^{-1})	7.46	7.99 ± 3.90	8.84	16.7 ± 13.9

larger than 1 mag are usually associated with eruptive variability (Scholz et al. 2013). Changes in the extinction along the line of sight can produce larger changes in the magnitudes and on longer timescales (Bouvier et al. 2013). However, the brightness variability of nearby stars is not significant and does not exceed ∼0.5 mag. This can be seen as an argument in favor of the fact that such a significant brightness increasing of UKIDSS-J185318.36+012454.5 did not occur as a result of the extinction variability. This conclusion is also supported by the MIR photometric data, namely, the measure flux increase at 21–22 μm. Hence, we can consider UKIDSS-J185318.36+012454.5 as an eruptive variable.

The increase in brightness, taking into account the photometric data in both NIR and MIR ranges, is likely to occur between 2004 and 2006. We note that Scholz et al. (2013) concluded that the objects may be candidates of the eruptive variables, in which the brightness at 3.6 and 4.5 μm bands increases by at least 1 mag. The brightness increase in the [3.6] band is indeed ∼1 mag, but in the [4.5] band it is lower, only ∼0.5 mag. We can assume that the first *Spitzer* data were just taken after the beginning of the outburst and while the YSO brightness still increased. Therefore we can logically conclude that the burst started between May 2003 and April 2004.

Cooper et al. (2013) presented the results of UKIDSS–J185318.36+012454.5 K-band spectroscopy. The observation was carried out after an outburst in 2007. The spectral data show H_2 2.1218 μm and CO emission. The emission of the Br series lines, as well as HeI 2.0587 μm emission, are below the limit of the detection sensitivity. The main spectral properties of FUors, which have a higher increase in luminosity and longer duration outbursts, generally display strong CO absorption and mostly lack emission lines in their IR spectra (Hartmann & Kenyon 1996). EXors-type objects, whose brightness increase is not as strong and whose outbursts are shoter, show strong emission of HI recombination lines, as well CO emission during the outburst (Herbig 2008). The increase in luminosity ($\Delta K_s > 5$ mag), outburst duration (NIR and MIR magnitudes show only slight fluctuations during about eight years), as well as the lack of Br series lines correspond to FUors. On the other hand, CO emission is one of the main characteristics of EXors. For comparison, we note that of the 19 eruptive variables from the list in Contreras Peña et al. (2017), Br series lines are not detected in only 4 cases (VVVv 322, 717, 721, and 815), but in contrast to our object, in the spectra of the first 3 objects, CO is observed in absorption. In spectra of the fourth, VVVv815, neither emission nor absorption is observed in the CO band. Thus, the spectral features of the objects have mixed characteristics of both FUors and Exors. We can offer the following explanation. According to the data presented in Shepherd et al. (2007), the G034.4+00.23 MM2 clump, where UKIDSS-J185318.36+012454.5 is located, is the source of the massive outflows observed in millimeter and MIR wavelengths. It cannot be excluded that the CO absorption of the stellar object is masked by very strong outflow emission. A similar situation is observed in the optical range in the spectra of FUor-type object V 2494 Cyg, where Hα absorption is masked by very strong and broad jet emission. Nevertheless, the summation of the observed photometric and spectral data does not allow us to classify UKIDSS-J185318.36+012454.5 a FUor

or an EXor. We can consider the object as an eruptive variable with mixed characteristics, namely, MNor.

Contradictory estimates of the distance of the star-forming region to which the object probably belongs complicate the determination of the mass and total luminosity. However, for both estimates of distances (the trigonometric maser parallax distance is 1.56 kpc and the kinematic distance is 3.7–3.9 kpc) we can classify UKIDSS-J185318.36+012454.5 as an intermediate-mass YSO with an age of $\sim 10^5$ yr. The ratio between the mass, total luminosity, and age of the object, as well as the disk accretion and envelope infall rates, correlates well within the error bars with several embedded eruptive variable YSOs presented in Contreras Peña et al. (2017).

5. Conclusion

On the basis of the infrared data and images, we have revealed the new eruptive variable UKIDSS−J185318.36+012454.5. According to the NIR and MIR colors and the SED of the object, we can classify it as a YSO with a Class 0/I evolution stage. It is located in the vicinity of IRAS 18507+0121 and probably belongs to the massive star-forming region associated with the UC H II region GAL 034.4+00.23. The outburst apparently occurred between May 2003 and April 2004. The brightness amplitude is at least $\Delta K_s = 5.0$ mag. At this brightness level, the object remained at least until 2014. The spectral observations carried out after the outburst show H_2 2.1218 μm and CO emission. The emission of the Br series lines is below the limit of the detector sensitivity. The summation of the photometric and spectral data does not allow us to classify UKIDSS−J185318.36+012454.5 as a FUor or EXor. We can consider it as an eruptive variable with mixed characteristics or an MNor-type object. According to the data obtained by the SED fitting tool, UKIDSS−J185318.36 + 012454.5 is an intermediate-mass YSO with an age of $\leq 10^5$ yr.

Acknowledgements. We are very grateful to the anonymous referee for helpful comments and suggestions. This research has made use of the data obtained at UKIRT which is supported by NASA and operated under an agreement of the University of Hawaii, the University of Arizona, and the Lockheed Martin Advanced Technology Center; operations are enabled through the cooperation of the East Asian Observatory. We gratefully acknowledge the use of data from the NASA/IPAC Infrared Science Archive, which is operated by the Jet Propulsion Laboratory, California Institute of Technology, under contract with the National Aeronautics and Space Administration. We thank the colleagues in the GLIMPSE I and DEEP GLIMPSE *Spitzer* Legacy Surveys. This paper is also based on observations taken as part of program 083.C–0846(A) which is operated by the European Southern Observatory.

References

Abrahamyan, H. V., Mickaelian, A. M., & Knyazyan, A. V. 2015, Astron. Comput., 10, 99
Allen, L. E., Calvet, N., D'Alessio, P., et al. 2004, ApJS, 154, 363
Allen, L., Megeath, S. T., Gutermuth, R., et al. 2007, Protostars and Planets V, 361
Aspin, C., & Reipurth, B. 2003, AJ, 126, 2936
Azatyan, N. M., Nikoghosyan, E. H., & Khachatryan, K. G. 2016, Astrophysics, 59, 339
Bans, A., & Königl, A. 2012, ApJ, 758, 100
Benjamin, R. A., Churchwell, E., Babler, B. L., et al. 2003, PASP, 115, 953
Bohlin, R. C., Savage, B. D., & Drake, J. F. 1978, ApJ, 224, 132
Bouvier, J., Grankin, K., Ellerbroek, L. E., Bouy, H., & Barrado, D. 2013, A&A, 557, A77
Churchwell, E., Babler, B. L., Meade, M. R., et al. 2009, PASP, 121, 213
Contreras Peña, C., Lucas, P. W., Froebrich, D., et al. 2014, MNRAS, 439, 1829
Contreras Peña, C., Lucas, P. W., Kurtev, R., et al. 2017, MNRAS, 465, 3039
Cooper, H. D. B., Lumsden, S. L., Oudmaijer, R. D., et al. 2013, MNRAS, 430, 1125
Cyganowski, C. J., Whitney, B. A., Holden, E., et al. 2008, AJ, 136, 2391
Edris, K. A., Fuller, G. A., & Cohen, R. J. 2007, A&A, 465, 865
Epchtein, N., Deul, E., Derriere, S., et al. 1999, A&A, 349, 236
Fazio, G. G., Hora, J. L., Allen, L. E., et al. 2004, ApJS, 154, 10
Flaherty, K. M., Pipher, J. L., Megeath, S. T., et al. 2007, ApJ, 663, 1069
Foster, J. B., Stead, J. J., Benjamin, R. A., Hoare, M. G., & Jackson, J. M. 2012, ApJ, 751, 157
Gramajo, L. V., Rodón, J. A., & Gómez, M. 2014, AJ, 147, 140
Grave, J. M. C., & Kumar, M. S. N. 2009, A&A, 498, 147
Gutermuth, R. A., Myers, P. C., Megeath, S. T., et al. 2008, ApJ, 674, 336
Harju, J., Lehtinen, K., Booth, R. S., & Zinchenko, I. 1998, A&AS, 132, 211
Hartmann, L., & Kenyon, S. J. 1996, ARA&A, 34, 207
Hartmann, L., Megeath, S. T., Allen, L., et al. 2005, ApJ, 629, 881
Herbig, G. H. 2008, AJ, 135, 637
Hodapp, K.-W., Hora, J. L., Rayner, J. T., Pickles, A. J., & Ladd, E. F. 1996, ApJ, 468, 861
Ishihara, D., Onaka, T., Kataza, H., et al. 2010, A&A, 514, A1
Kurayama, T., Nakagawa, A., Sawada-Satoh, S., et al. 2011, PASJ, 63, 513
Lada, C. J., & Lada, E. A. 2003, ARA&A, 41, 57
Lucas, P. W., Hoare, M. G., Longmore, A., et al. 2008, MNRAS, 391, 136
Lumsden, S. L., Hoare, M. G., Urquhart, J. S., et al. 2013, ApJS, 208, 11
Miralles, M. P., Rodriguez, L. F., & Scalise, E. 1994, ApJS, 92, 173
Molinari, S., Brand, J., Cesaroni, R., & Palla, F. 1996, A&A, 308, 573
Molinari, S., Schisano, E., Elia, D., et al. 2016, A&A, 591, A149
Moorwood, A., Cuby, J.-G., & Lidman, C. 1998, The Messenger, 91, 9
Morales, E. F. E., Wyrowski, F., Schuller, F., & Menten, K. M. 2013, A&A, 560, A76
Persi, P., Tapia, M., Gòmez, M., et al. 2007, AJ, 133, 1690
Rathborne, J. M., Jackson, J. M., Chambers, E. T., et al. 2005, ApJ, 630, L181
Reach, W. T., Megeath, S. T., Cohen, M., et al. 2005, PASP, 117, 978
Reipurth, B., Aspin, C., Beck, T., et al. 2007, AJ, 133, 1000
Rieke, G. H., & Lebofsky, M. J. 1985, ApJ, 288, 618
Robitaille, T. P., Whitney, B. A., Indebetouw, R., & Wood, K. 2007, ApJS, 169, 328
Schlegel, D. J., Finkbeiner, D. P., & Davis, M. 1998, ApJ, 500, 525
Scholz, A., Xu, X., Jayawardhana, R., et al. 2009, MNRAS, 398, 873
Scholz, A., Froebrich, D., & Wood, K. 2013, MNRAS, 430, 2910
Shepherd, D. S., Nürnberger, D. E. A., & Bronfman, L. 2004, ApJ, 602, 850
Shepherd, D. S., Povich, M. S., Whitney, B. A., et al. 2007, ApJ, 669, 464
Simon, R., Rathborne, J. M., Shah, R. Y., Jackson, J. M., & Chambers, E. T. 2006, ApJ, 653, 1325
Skrutskie, M. F., Cutri, R. M., Stiening, R., et al. 2006, AJ, 131, 1163
Szymczak, M., Hrynek, G., & Kus, A. J. 2000, A&AS, 143, 269
Varricatt, W. P., Davis, C. J., Ramsay, S., & Todd, S. P. 2010, MNRAS, 404, 661
Vijh, U. P., Meixner, M., Babler, B., et al. 2009, AJ, 137, 3139
Whitney, B., Benjamin, R., Churchwell, E., et al. 2011, Deep GLIMPSE: Exploring the Far Side of the Galaxy, Spitzer Proposal, 80074
Xu, J.-L., Li, D., Zhang, C.-P., et al. 2016, ApJ, 819, 117
Xue, M., Jiang, B. W., Gao, J., et al. 2016, ApJS, 224, 23